Aalto University

OPEN ACCESS

This is an electronic reprint of the original article.
This reprint may differ from the original in pagination and typographic detail.

Awan, Hafiz Asad Ali; Hinkkanen, Marko; Bojoi, Radu; Pellegrino, Gianmario

Stator-flux-oriented control of synchronous motors

Published in:
IEEE Transactions on Industry Applications

DOI:
10.1109/TIA.2019.2927316

Published: 09/07/2019

Document Version
Peer-reviewed accepted author manuscript, also known as Final accepted manuscript or Post-print

Please cite the original version:
Awan, H. A. A., Hinkkanen, M., Bojoi, R., & Pellegrino, G. (2019). Stator-flux-oriented control of synchronous motors: A systematic design procedure. *IEEE Transactions on Industry Applications*, *55*(5), 4811-4820. https://doi.org/10.1109/TIA.2019.2927316

This material is protected by copyright and other intellectual property rights, and duplication or sale of all or part of any of the repository collections is not permitted, except that material may be duplicated by you for your research use or educational purposes in electronic or print form. You must obtain permission for any other use. Electronic or print copies may not be offered, whether for sale or otherwise to anyone who is not an authorised user.

Stator-Flux-Oriented Control of Synchronous Motors: A Systematic Design Procedure

Hafiz Asad Ali Awan, Marko Hinkkanen, *Senior Member, IEEE*, Radu Bojoi, *Fellow, IEEE*, and Gianmario Pellegrino, *Senior Member, IEEE*

***Abstract*—This paper deals with stator-flux-oriented control of permanent-magnet (PM) synchronous motors and synchronous reluctance motors (SyRMs). The variables to be controlled are the stator-flux magnitude and the torque-producing current component, whose references are easy to calculate. However, the dynamics of these variables are nonlinear and coupled, potentially compromising the control performance. We propose an exact input-output feedback linearization structure and a systematic design procedure for the stator-flux-oriented control method in order to improve the control performance. The proposed controller is evaluated by means of experiments using a 6.7-kW SyRM drive and a 2.2-kW interior PM synchronous motor drive.**

***Index Terms*—Input-output feedback linearization, nonlinear control, permanent-magnet synchronous motor, stator-flux-oriented control, synchronous reluctance motor.**

I. Introduction

SYNCHRONOUS reluctance motors (SyRMs) with or without permanent magnets (PMs) provide the high torque density and good flux-weakening capability. Under optimal control, these motors operate along the maximum-torque-per-ampere (MTPA) locus, in the field-weakening region, or at the maximum-torque-per-volt (MTPV) limit, depending on the operating speed and the torque reference [1].

Chiefly, torque control methods are based on controlling the current components i_d and i_q in rotor coordinates [2]–[6]. A linear current controller, equipped with pulse-width modulation (PWM) and synchronous sampling of the currents, is typically used [7]–[11]. If the magnetic saturation and the speed changes are omitted, the dynamics seen by the current controller are linear and the closed-loop system can be made comparatively robust [8]. The optimal current references can be fetched from pre-computed look-up tables [2]–[6]. In addition to one-dimensional MTPA and MTPV tables, at least one two-dimensional look-up table is typically needed.

Direct torque control (DTC) is an alternative to current vector control [12]–[15]. The stator-flux magnitude and the electromagnetic torque are controlled by means of hysteresis controllers. DTC does not use PWM, and the switching frequency is not constant. Furthermore, since there is no current control loop, the current limitation relies on torque reference limitation, which is, in turn, parameter-dependent.

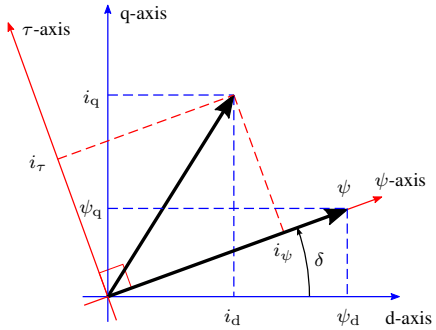

Fig. 1. Rotor coordinates (dq) and stator flux coordinates ($\psi\tau$). Flux and current components are depicted in both coordinates.

In stator-flux-oriented control [16], [17] and in its variant called direct-flux vector control (DFVC) [18], [19], the stator-flux magnitude ψ and the torque-producing current i_τ are selected as the controlled variables, cf. Fig. 1. This choice simplifies calculation of the references. Only the MTPA and MTPV features have to be implemented, but no two-dimensional look-up tables are needed. Conventionally, two separately tuned proportional-integral (PI) controllers are used for controlling the stator-flux magnitude and the torque-producing current component [16]–[19]. Instead of the torque-producing current component, it is also possible to control the electromagnetic torque directly [20], [21]. Unlike DTC, stator-flux-oriented control employs PWM. Furthermore, the currents are sampled in synchronism with PWM. Therefore, the switching harmonics in the currents (and in the torque) are similar to those in the current-controlled drives.

A drawback of the stator-flux-oriented schemes is that the torque-producing current control loop is nonlinear (even in the case of linear magnetics), which complicates the tuning procedure. The control performance for constant gains depends on the operating point due to the nonlinear dynamics. To avoid an oscillatory response, the control design can be performed for the best case in a suboptimal manner [18].

In this paper, we develop a feedback-linearization stator-flux-oriented control method and its systematic design procedure. The reference calculation methods are left out of the scope, but the proposed control method is directly compatible

Conference version "Stator-flux-oriented control of synchronous motors: design and implementation" of this paper was presented at the 2018 IEEE Energy Conversion Congress and Exposition (ECCE), Portland, OR, Sep. 23–27. This work was supported by ABB Oy Drives.

H. A. A. Awan is with ABB Oy Drives, Helsinki, Finland (email: asad.awan@fi.abb.com).

M. Hinkkanen is with the Department of Electrical Engineering and Automation, Aalto University, Espoo, Finland (e-mail: marko.hinkkanen@aalto.fi).

R. Bojoi and G. Pellegrino are with the Department of Electrical Engineering, Politecnico di Torino, Turin, Italy (e-mail: radu.bojoi@polito.it; gianmario.pellegrino@polito.it).

with the available methods [6], [18], [19]. After introducing the motor model in Section II, the control structure and the main contributions are presented in Section III:

1) An exact input-output feedback linearization controller structure is derived, yielding a completely decoupled and easy-to-tune system.
2) Design guidelines and tuning principles are presented.
3) An anti-windup mechanism is developed, taking into account the nonlinear structure of the controller.

In Section IV, the dynamic performance of the proposed control method is studied by means of experiments, using a motion-sensored 6.7-kW SyRM drive and a motion-sensorless 2.2-kW interior PM synchronous motor drive. In Section V, the parameter sensitivity of the proposed method is studied, and a discussion of its advantages and disadvantages is provided. A preliminary version of this paper was presented in a conference [22].

II. Motor Model

A. Rotor Coordinates

A standard model for PM synchronous motors is used, expressed using real space vectors. As an example, the stator flux linkage in rotor coordinates is denoted by $\boldsymbol{\psi} = [\psi_\mathrm{d}, \psi_\mathrm{q}]^\mathrm{T}$, where ψ_d and ψ_q are the direct and quadrature components, respectively. The stator voltage equation is

$$\frac{\mathrm{d}\boldsymbol{\psi}}{\mathrm{d}t} = \boldsymbol{u} - R\boldsymbol{i} - \omega_\mathrm{m}\mathbf{J}\boldsymbol{\psi} \tag{1}$$

where $\boldsymbol{u}$ is the stator voltage, $\boldsymbol{i}$ is the stator current, R is the stator resistance, ω_m is the electrical angular speed of the rotor, and $\mathbf{J} = \left[\begin{smallmatrix} 0 & -1 \\ 1 & 0 \end{smallmatrix}\right]$ is the orthogonal rotation matrix. The stator flux is

$$\boldsymbol{\psi} = \boldsymbol{L}\boldsymbol{i} + \boldsymbol{\psi}_\mathrm{f} \tag{2}$$

The inductance matrix and the PM-flux vector, respectively, are

$$\boldsymbol{L} = \begin{bmatrix} L_\mathrm{d} & 0 \\ 0 & L_\mathrm{q} \end{bmatrix} \qquad \boldsymbol{\psi}_\mathrm{f} = \begin{bmatrix} \psi_\mathrm{f} \\ 0 \end{bmatrix} \tag{3}$$

where L_d is the d-axis inductance, L_q is the q-axis inductance, and ψ_f is the flux linkage induced due to the PMs. If $L_\mathrm{d} = L_\mathrm{q}$, the model represents a surface-mounted PM motor. If $\psi_\mathrm{f} = 0$, the model of an SyRM is obtained. The electromagnetic torque can be written as

$$T = \frac{3p}{2}\boldsymbol{i}^\mathrm{T}\mathbf{J}\boldsymbol{\psi} = \frac{3p}{2}(\psi_\mathrm{d} i_\mathrm{q} - \psi_\mathrm{q} i_\mathrm{d}) \tag{4}$$

where p is the number of pole pairs.

B. Stator Flux Coordinates

Fig. 1 shows stator flux coordinates ($\psi\tau$), whose ψ-axis is parallel to the stator flux vector. The vectors in these coordinates are marked with the superscript f, e.g.,

$$\boldsymbol{\psi}^\mathrm{f} = \begin{bmatrix} \psi \\ 0 \end{bmatrix} = \mathrm{e}^{-\delta\mathbf{J}}\boldsymbol{\psi} \qquad \boldsymbol{i}^\mathrm{f} = \begin{bmatrix} i_\psi \\ i_\tau \end{bmatrix} = \mathrm{e}^{-\delta\mathbf{J}}\boldsymbol{i} \tag{5}$$

where δ is the angle of the stator flux vector in rotor coordinates.[1] Other vectors are transformed to stator flux coordinates similarly. In these coordinates, the torque expression (4) reduces to

$$T = \frac{3p}{2}\psi i_\tau \tag{6}$$

As explained later, reference calculation becomes simple, if the stator-flux magnitude ψ and the torque-producing current i_τ are used as the controlled state variables. These variables are packed into a state vector

$$\boldsymbol{x}^\mathrm{f} = \begin{bmatrix} \psi \\ i_\tau \end{bmatrix} \tag{7}$$

Using (1), (2), and (5), a nonlinear model with the desired state variables is obtained [18]

$$\frac{\mathrm{d}\boldsymbol{x}^\mathrm{f}}{\mathrm{d}t} = \begin{bmatrix} 1 & 0 \\ a/L_\mathrm{d} & b/L_\mathrm{d} \end{bmatrix}\left(\boldsymbol{u}^\mathrm{f} - R\boldsymbol{i}^\mathrm{f} - \omega_\mathrm{m}\mathbf{J}\boldsymbol{\psi}^\mathrm{f}\right) \tag{8}$$

where the factors are

$$\begin{aligned} a &= \frac{1}{2}\left(\frac{L_\mathrm{d}}{L_\mathrm{q}} - 1\right)\sin 2\delta \\ b &= \frac{\psi_\mathrm{f}}{\psi}\cos\delta + \left(\frac{L_\mathrm{d}}{L_\mathrm{q}} - 1\right)\cos 2\delta \end{aligned} \tag{9}$$

It is to be noted that the condition $b = 0$ corresponds to the MTPV limit [16].

III. Control Design

A. Structure of the Control System

Fig. 2(a) shows the overall structure of the control system considered in this paper. The measured current is transformed to rotor coordinates using the electrical angle ϑ_m of the rotor. The voltage reference $\boldsymbol{u}_\mathrm{ref}$ is transformed to stator coordinates, marked with the superscript s, and fed to PWM. The main focus of this paper is on the stator-flux-oriented controller, which controls the state variables defined in (7). This choice of the state variables is advantageous since the optimal reference $\boldsymbol{x}^\mathrm{f}_\mathrm{ref} = [\psi_\mathrm{ref}, i_{\tau,\mathrm{ref}}]^\mathrm{T}$ is comparatively easy to calculate from the torque reference T_ref, the measured speed ω_m, and the measured DC-bus voltage u_dc.

The proposed stator-flux-oriented controller is directly compatible with the existing reference calculation methods, such as [6], [18], [19]. Fig. 2(b) shows the feedforward reference calculation method [6], which is applied in the experiments of this paper. For the sake of completeness, this method is briefly described in the following. Due to the feedforward nature of the reference calculation method in Fig. 2(b), the dynamics of the inner control loop remain intact and the noise content in the state references is minor. The MTPA and MTPV tables can be computed automatically, if the magnetic model of the motor is known [6].

The reference calculation method in Fig. 2(b) can be used in current-controlled drives as well [3], [6]. However, one or two additional two-dimensional look-up tables (depending on

[1] For brevity, the coordinate transformations are expressed using the matrix exponential. The transformation can be written as $\exp(\delta\mathbf{J}) = \left[\begin{smallmatrix} \cos\delta & -\sin\delta \\ \sin\delta & \cos\delta \end{smallmatrix}\right]$. The matrix elements are $\cos\delta = \psi_\mathrm{d}/\psi$ and $\sin\delta = \psi_\mathrm{q}/\psi$, where the flux magnitude is $\psi = (\psi_\mathrm{d}^2 + \psi_\mathrm{q}^2)^{1/2}$.

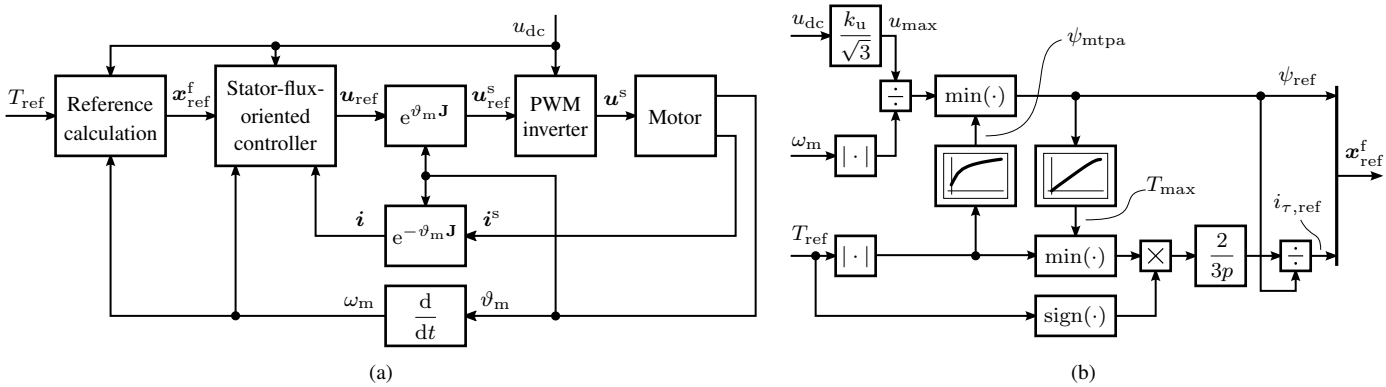

Fig. 2. Control system: (a) overall block diagram; (b) reference calculation. In (b), one look-up table gives the optimal flux ψ_{mtpa} corresponding to the MTPA locus and the other gives the maximum torque T_{max} corresponding to the MTPV and current limits. The maximum steady-state voltage u_{max} is obtained from the DC-bus voltage u_{dc}. The factor k_{u} defines the voltage margin.

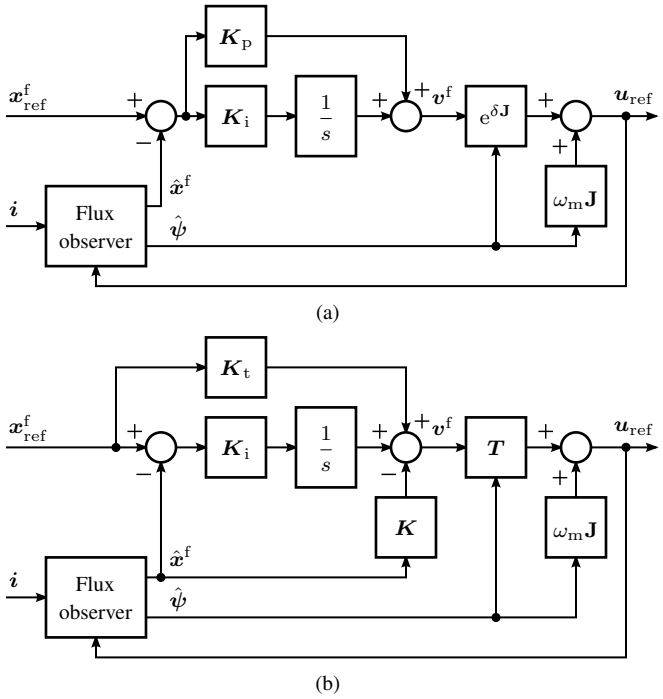

Fig. 3. Stator-flux-oriented controller: (a) conventional method; (b) proposed method. The nonlinear transformation matrix $\boldsymbol{T} = \boldsymbol{T}(\boldsymbol{\psi})$ is given in (20). Here, the flux observer operates in rotor coordinates, but stator coordinates could be used as well. The compensation for the resistive voltage drop has been omitted. The anti-windup is not shown in these figures.

the implementation) are needed for transforming $\boldsymbol{x}^{\mathrm{f}}_{\mathrm{ref}}$ to the corresponding optimal current reference $\boldsymbol{i}_{\mathrm{ref}}$. This additional complexity is avoided in stator-flux-oriented control.

It is worth noticing that the MTPV limit as well as the zero-flux condition are singularities in stator-flux-oriented control. Therefore, a small margin (e.g. 5…10%) in the MTPV limit and a small minimum value for ψ_{ref} are needed in the implementation. In the case of current-controlled drives, these singularities do not exist.

B. Conventional Stator-Flux-Oriented Controller

Fig. 3(a) shows a conventional stator-flux-oriented controller similar to [18], [19]. Its two key elements, a flux observer and a PI controller are briefly reviewed in the following. An ideal PWM inverter is assumed, $\boldsymbol{u} = \boldsymbol{u}_{\mathrm{ref}}$.

1) Flux Observer: The stator-flux-oriented controller needs an estimate of the stator flux $\boldsymbol{\psi}$. The flux can be estimated directly using the flux model (2) without any observer. Then, the state vector $\boldsymbol{x}^{\mathrm{f}}$ is obtained using (5) and (7). An advantage of this approach is that the order of the whole control system is not increased due to the flux estimation and no additional gains are needed.

Applying a flux observer is preferred in practice, since it reduces the sensitivity to the errors in the magnetic model (2) and to the measurement noise. If the drive is equipped with a position sensor, the flux linkage can be estimated using a simple state observer in rotor coordinates,

$$\frac{\mathrm{d}\hat{\boldsymbol{\psi}}}{\mathrm{d}t} = \boldsymbol{u} - R\boldsymbol{i} - \omega_{\mathrm{m}}\mathbf{J}\hat{\boldsymbol{\psi}} + \boldsymbol{G}(\boldsymbol{L}\boldsymbol{i} + \boldsymbol{\psi}_{\mathrm{f}} - \hat{\boldsymbol{\psi}}) \tag{10}$$

where $\boldsymbol{G}$ is the observer gain matrix. Based on (1), (2), and (10), the dynamics of the estimation error $\tilde{\boldsymbol{\psi}} = \boldsymbol{\psi} - \hat{\boldsymbol{\psi}}$ are governed by

$$\frac{\mathrm{d}\tilde{\boldsymbol{\psi}}}{\mathrm{d}t} = -\left(\omega_{\mathrm{m}}\mathbf{J} + \boldsymbol{G}\right)\tilde{\boldsymbol{\psi}} \tag{11}$$

Therefore, any desired closed-loop system matrix can be easily set via the observer gain $\boldsymbol{G}$. If a constant gain matrix $\boldsymbol{G} = g\mathbf{I}$ is used, the observer behaves as the voltage model at higher speeds and as the flux model at low speeds [23]. The parameter g defines the corner frequency (typically $g = 2\pi \cdot 15 \ldots 30$ rad/s). The flux observer (10) is presented here as an example, but other flux observers could be used instead. For enabling sensorless operation, observers reviewed in [24] can be applied.

According to Fig. 3, the estimated state vector $\hat{\boldsymbol{x}}^{\mathrm{f}}$ is controlled. This vector is defined as

$$\hat{\boldsymbol{x}}^{\mathrm{f}} = \begin{bmatrix} \hat{\psi} \\ i_\tau \end{bmatrix} = \begin{bmatrix} \sqrt{\hat{\psi}_{\mathrm{d}}^2 + \hat{\psi}_{\mathrm{q}}^2} \\ -i_{\mathrm{d}}\sin\delta + i_{\mathrm{q}}\cos\delta \end{bmatrix} \tag{12}$$

where the stator flux angle δ is calculated using the estimated flux components $\hat{\psi}_{\mathrm{d}}$ and $\hat{\psi}_{\mathrm{q}}$. If needed, the torque estimate

$$\hat{T} = \frac{3p}{2}\hat{\psi} i_\tau \tag{13}$$

can be easily calculated.

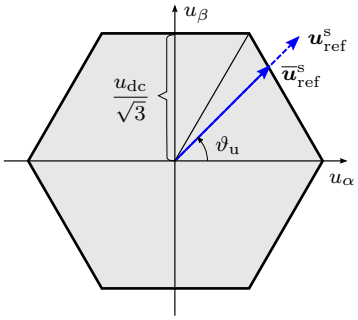

Fig. 4. Voltage hexagon of a two-level PWM inverter in stator coordinates.

2) PI Controller: As shown in Fig. 3(a), the voltage reference in rotor coordinates is

$$\boldsymbol{u}_{\mathrm{ref}} = R\boldsymbol{i} + \omega_{\mathrm{m}}\mathbf{J}\boldsymbol{\psi} + \mathrm{e}^{\delta\mathbf{J}}\boldsymbol{v}^{\mathrm{f}} \tag{14}$$

The output of the PI controller is

$$\boldsymbol{v}^{\mathrm{f}} = \left(\boldsymbol{K}_{\mathrm{p}} + \frac{\boldsymbol{K}_{\mathrm{i}}}{s}\right)\left(\boldsymbol{x}^{\mathrm{f}}_{\mathrm{ref}} - \boldsymbol{x}^{\mathrm{f}}\right) \tag{15}$$

where $s = \mathrm{d}/\mathrm{d}t$ is used as the differential operator. The gain matrices are

$$\boldsymbol{K}_{\mathrm{p}} = \begin{bmatrix} k_{\mathrm{p}\psi} & 0 \\ 0 & k_{\mathrm{p}\tau} \end{bmatrix} \qquad \boldsymbol{K}_{\mathrm{i}} = \begin{bmatrix} k_{\mathrm{i}\psi} & 0 \\ 0 & k_{\mathrm{i}\tau} \end{bmatrix} \tag{16}$$

where $k_{\mathrm{p}\psi}$ and $k_{\mathrm{i}\psi}$ are the gains for the flux channel and $k_{\mathrm{p}\tau}$ and $k_{\mathrm{i}\tau}$ are the gains for the torque channel. The effect of the compensation for the resistive voltage drop in (14) is small and it can be omitted due to the integral action in (15).

Typically, constant gains are used in (16). As mentioned, the motor model in (8) is nonlinear and the dynamics of i_τ depend strongly on b [18]. Therefore, the control response for constant gains depends on the operating point.

C. Proposed Stator-Flux-Oriented Controller

Fig. 3(b) shows the proposed stator-flux-oriented controller, which is explained in the following. The same flux observer as in the conventional method can be used.

1) Nonlinear State Feedback: We apply exact input-output feedback linearization [25] to tackle the nonlinearity in the model (8). Inserting the control law[2]

$$\boldsymbol{u}^{\mathrm{f}}_{\mathrm{ref}} = R\boldsymbol{i}^{\mathrm{f}} + \omega_{\mathrm{m}}\mathbf{J}\boldsymbol{\psi}^{\mathrm{f}} + \begin{bmatrix} 1 & 0 \\ -a/b & L_{\mathrm{d}}/b \end{bmatrix}\boldsymbol{v}^{\mathrm{f}} \tag{17}$$

into (8) leads to a simple linear system

$$\frac{\mathrm{d}\boldsymbol{x}^{\mathrm{f}}}{\mathrm{d}t} = \boldsymbol{v}^{\mathrm{f}} \tag{18}$$

where $\boldsymbol{v}^{\mathrm{f}}$ is the transformed input vector, obtained from an external linear controller to be designed in the following. The control law (17) can be transformed to rotor coordinates, leading to

$$\boldsymbol{u}_{\mathrm{ref}} = R\boldsymbol{i} + \omega_{\mathrm{m}}\mathbf{J}\boldsymbol{\psi} + \boldsymbol{T}\boldsymbol{v}^{\mathrm{f}} \tag{19}$$

[2]The voltage inputs u_ψ and u_τ appear in the outputs ψ and i_τ in (5) after one differentiation, the relative degree of both outputs is one, and the total relative degree is $r = 2$. The order of the system is $n = 2$. Since $n - r = 0$, there are no zero dynamics and the system is fully input-output linearizable [25].

where

$$\boldsymbol{T} = \mathrm{e}^{\delta\mathbf{J}}\begin{bmatrix} 1 & 0 \\ -a/b & L_{\mathrm{d}}/b \end{bmatrix} \tag{20}$$

This nonlinear transformation matrix includes both the coordinate transformation (from stator flux coordinates to rotor coordinates) and the feedback linearization.

2) Linear Controller: The relation (18) between the transformed input and the output can be rewritten as

$$\boldsymbol{x}^{\mathrm{f}} = \boldsymbol{v}^{\mathrm{f}}/s \tag{21}$$

Any linear controller can be easily designed for the system (21). As an example, a simple proportional controller would suffice, if steady-state errors were acceptable. Here, a state-feedback controller with reference feedforward and integral action is used,

$$\boldsymbol{v}^{\mathrm{f}} = \boldsymbol{K}_{\mathrm{t}}\boldsymbol{x}^{\mathrm{f}}_{\mathrm{ref}} + \frac{\boldsymbol{K}_{\mathrm{i}}}{s}\left(\boldsymbol{x}^{\mathrm{f}}_{\mathrm{ref}} - \boldsymbol{x}^{\mathrm{f}}\right) - \boldsymbol{K}\boldsymbol{x}^{\mathrm{f}} \tag{22}$$

where $\boldsymbol{K}_{\mathrm{t}}$ is the reference-feedforward gain, $\boldsymbol{K}_{\mathrm{i}}$ is the integral gain, and $\boldsymbol{K}$ is the state-feedback gain. The gains can be selected as $\boldsymbol{K}_{\mathrm{t}} = \alpha\mathbf{I}$, $\boldsymbol{K}_{\mathrm{i}} = \alpha^2\mathbf{I}$, and $\boldsymbol{K} = 2\alpha\mathbf{I}$, leading to the first-order closed-loop response

$$\boldsymbol{x}^{\mathrm{f}} = \frac{\alpha}{s+\alpha}\boldsymbol{x}^{\mathrm{f}}_{\mathrm{ref}} \tag{23}$$

where α is the bandwidth. If desired, the controller could be easily modified such that the flux and torque channels have different bandwidths. It is worth noticing that the effects of the parameter errors in the nonlinear transformation (20) on the steady-state accuracy are compensated for by the integral action of the linear controller (22).

As can be seen from Fig. 3(b), the structure of the proposed controller is similar to the conventional controller. The computational burden of the proposed controller is comparable to the conventional controller. Unlike in the case of the conventional controller, the control response is independent of the operating point. Furthermore, the proposed controller is easier to tune, since only the desired closed-loop bandwidth is needed (in addition to the motor parameters, which are needed in any case for the observer). The proposed controller is also more robust against parameter errors than the conventional controller, as discussed later in Section V.

3) Anti-Windup Scheme: So far, we have assumed an ideal inverter, $\boldsymbol{u} = \boldsymbol{u}_{\mathrm{ref}}$. Since the inverter output voltage is limited in reality, the control system requires an anti-windup technique in order to prevent integrator windup. Fig. 4 illustrates the maximum available voltage, which corresponds to the border of the voltage hexagon. In the first sector, the maximum voltage magnitude is [26]

$$u_{\max} = \frac{u_{\mathrm{dc}}}{\sqrt{3}\sin(2\pi/3 - \vartheta_{\mathrm{u}})} \tag{24}$$

where $\vartheta_{\mathrm{u}} = [0, \pi/3]$ is the angle of the voltage reference $\boldsymbol{u}^{\mathrm{s}}_{\mathrm{ref}}$. This equation can be easily applied in other sectors as well. The realizable voltage reference can be calculated as

$$\overline{\boldsymbol{u}}_{\mathrm{ref}} = \begin{cases} \boldsymbol{u}_{\mathrm{ref}}, & \text{if } \|\boldsymbol{u}_{\mathrm{ref}}\| \le u_{\max} \\ \dfrac{\boldsymbol{u}_{\mathrm{ref}}}{\|\boldsymbol{u}_{\mathrm{ref}}\|}u_{\max}, & \text{if } \|\boldsymbol{u}_{\mathrm{ref}}\| > u_{\max} \end{cases} \tag{25}$$

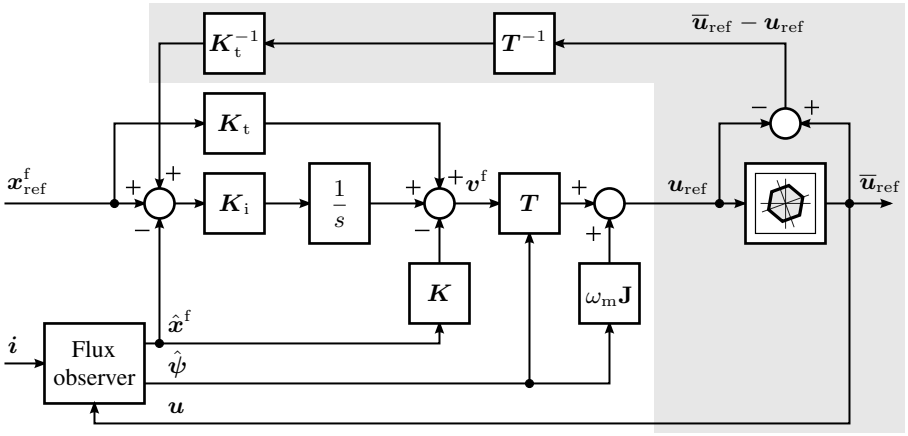

Fig. 5. Stator-flux-oriented controller, including an anti-windup scheme (shaded region). This structure is valid also for the conventional method, if $\boldsymbol{T} = \exp(\delta\mathbf{J})$ and $\boldsymbol{K}_\mathrm{t} = \boldsymbol{K} = \boldsymbol{K}_\mathrm{p}$ are used.

The realizable voltage can be either calculated in the controller using (24) and (25) or obtained from PWM.

Fig. 5 shows the stator-flux-oriented controller equipped with an anti-windup technique, which is based on the realizable reference [27]. It is important to notice that the effect of the nonlinear transformation in (20) has to be properly included in the anti-windup scheme, as shown in the figure.

IV. Experimental Results

The proposed stator-flux-oriented controller, shown in Figs. 2 and 5, is evaluated by means of experiments, using a 6.7-kW four-pole SyRM and a 2.2-kW six-pole interior PM synchronous motor (cf. the Appendix). The controller was discretized using the forward Euler method and implemented on a dSPACE processor board. Single-update PWM is used, and the sampling (switching) frequency is 5 kHz. The stator currents and the DC-link voltage are measured in synchronism with PWM. The desired closed-loop bandwidth is $\alpha = 2\pi \cdot 100$ rad/s. Unless otherwise noted, the flux observer (10) is used.

The conventional stator-flux-oriented controller is used as a benchmark method. It is obtained from the controller in Fig. 5, when $\boldsymbol{T} = \exp(\delta\mathbf{J})$ and $\boldsymbol{K}_\mathrm{t} = \boldsymbol{K} = \boldsymbol{K}_\mathrm{p}$ are chosen. For the 6.7-kW SyRM, the gains in (16) are $k_{\mathrm{p}\psi} = 628$ rad/s, $k_{\mathrm{i}\psi} = 21$ (rad/s)^2, $k_{\mathrm{p}\tau} = 628$ V/A, and $k_{\mathrm{i}\tau} = 21$ V/(As). According to [18], these gains correspond to the best-case design bandwidth of $2\pi \cdot 100$ rad/s.

A. Torque Reference Steps at Zero Speed

The 6.7-kW SyRM drive is controlled in the torque-control mode and the speed is maintained at zero by locking the rotor. The torque reference is stepped from 0 to the rated torque with increments of 25% of the rated torque. Fig. 6(a) shows the results for the conventional controller. As expected due to the nonlinear dynamics (8), the control response depends on the operating point and overshoots appear in the controlled variables. The control performance could be improved by means of scheduling the controller gains as a function of the operating point. However, the gain scheduling would be a difficult and time-consuming process, if performed by means of the trial-and-error method. Fig. 6(b) shows the results for the proposed controller. It can be seen that the control response is independent of the operating point and there is no overshoot in the controlled variables.

Fig. 7 shows the zoomed-in waveforms from the first torque step in Fig. 6. The control response is poorly damped in the case of the conventional controller. On the other hand, the response of the proposed controller matches well with the desired first-order response, cf. (23), the minor differences originating from the magnetic saturation characteristics of the SyRM.

B. Acceleration Test

The control scheme shown in Fig. 2 is augmented with the speed controller, which provides the torque reference T_ref based on the speed reference $\omega_{\mathrm{m,ref}}$ and the measured speed ω_m. Fig. 8 shows the results of the acceleration test, where the speed reference is changed stepwise from 0 to 2 p.u. at $t = 0.5$ s. The current limit is 1.5 p.u. In the case of the conventional controller, significant overshoots appear in the controlled variables at $t = 0.5$ s. In the case of the proposed controller, the controlled variables follow their references with no overshoot.[3]

Fig. 9 shows the measured phase current samples from the acceleration test in Fig. 8, with a zoomed-in time scale. The PWM harmonics are not present in the synchronously sampled currents. The remaining harmonics originate mainly from spatially nonuniform saturation (of the SyRM stator) and from operation at the boundary of the overmodulation region. Overall, the harmonic distortion of the currents is similar to the current-controlled drives, cf. e.g., the results in [10].

To test the performance of the proposed controller in sensorless operation, the observer (10) is replaced with a sensorless flux observer and the speed estimate is fed to the speed controller [24]. The studied motor is the 2.2-kW interior

[3]In Fig. 8, the torque-producing current component i_τ increases in the beginning of the field-weakening operation while the flux magnitude decreases. The current i_τ is bounded by the current limit and by the MTPV limit according to Fig. 2(b). The decrease in the flux-producing current i_ψ enables the increase in i_τ, until the MTPV limit is reached.

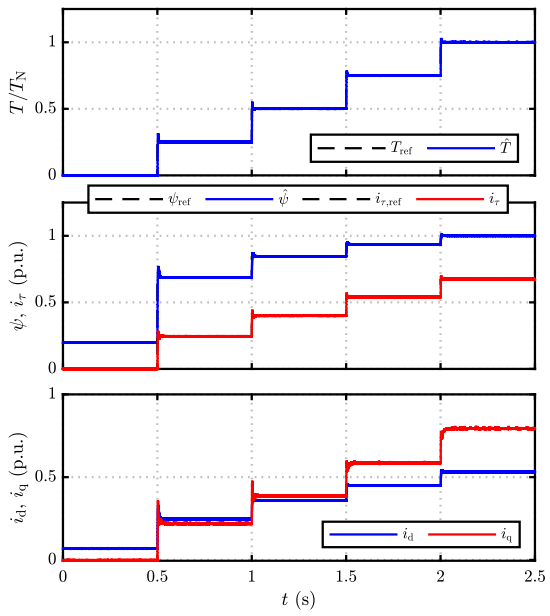

(a) Conventional controller.

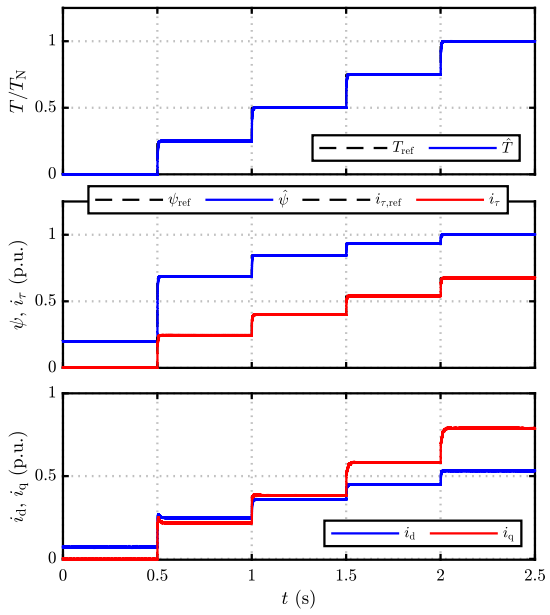

(b) Proposed controller.

Fig. 6. Experimental results for the 6.7-kW SyRM: (a) conventional controller; (b) proposed controller. The torque reference is changed stepwise at zero speed. First subplot: torque reference and torque estimate (13). Second subplot: controlled variables and their references. Last subplot: measured current components in rotor coordinates.

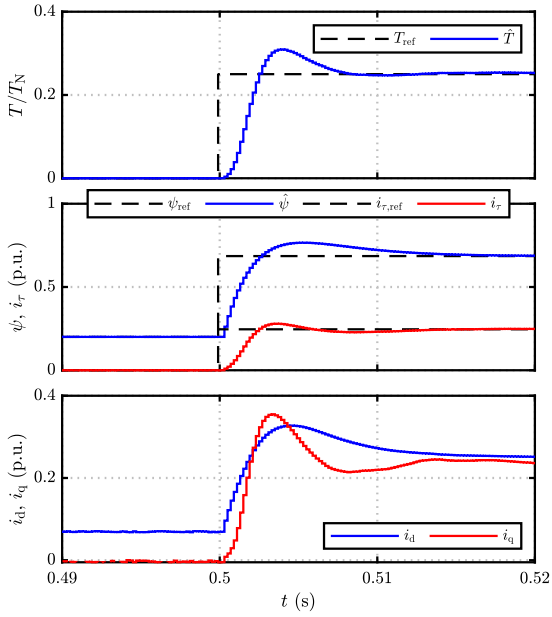

(a) Conventional controller.

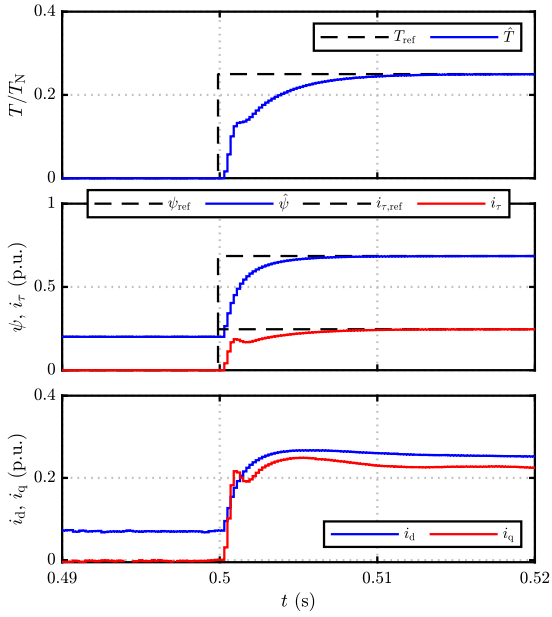

(b) Proposed controller.

Fig. 7. Zoomed-in waveforms from Fig. 6: (a) conventional controller; (b) proposed controller. The staircase waveforms are due to the sampling frequency of 5 kHz used in the control system.

PM synchronous motor. As an example, the results of the acceleration test are shown in Fig. 10. It can be seen that the estimated speed follows the measured one and the estimated states follow their references.

V. Discussion

Only experimental results were shown in the previous section. Here, robustness aspects are studied by means of simulations, and the advantages and disadvantages of stator-flux-oriented control are summarized.

A. Robustness Comparison

The robustness of the conventional and proposed stator-flux-oriented controllers against parameter errors is compared by means of simulations. The flux observer (10) is used. The parameter estimates of the 2.2-kW interior PM motor, given in the Appendix, are used in the control system, and the errors are introduced in the plant model. For the conventional controller, the gains are $k_{\mathrm{p}\psi} = 628$ rad/s, $k_{\mathrm{i}\psi} = 21$ (rad/s)^2, $k_{\mathrm{p}\tau} = 628$ V/A, and $k_{\mathrm{i}\tau} = 21$ V/(As), corresponding to the best-case design bandwidth of $2\pi \cdot 100$ rad/s.

The motor operates at the constant speed of $\omega_\mathrm{m} = 0.75$

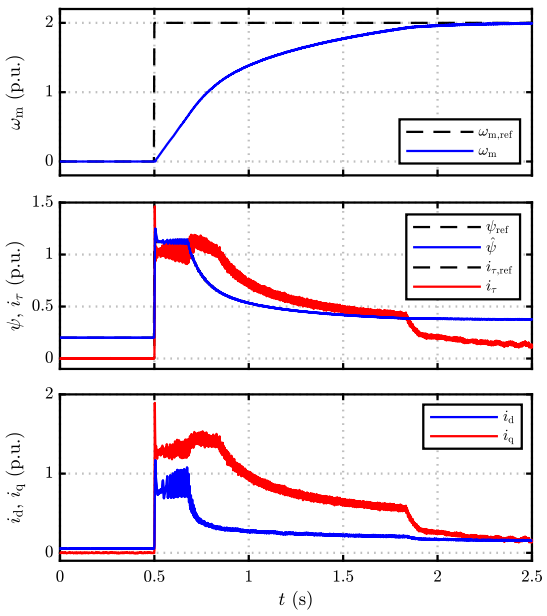

(a) Conventional controller.

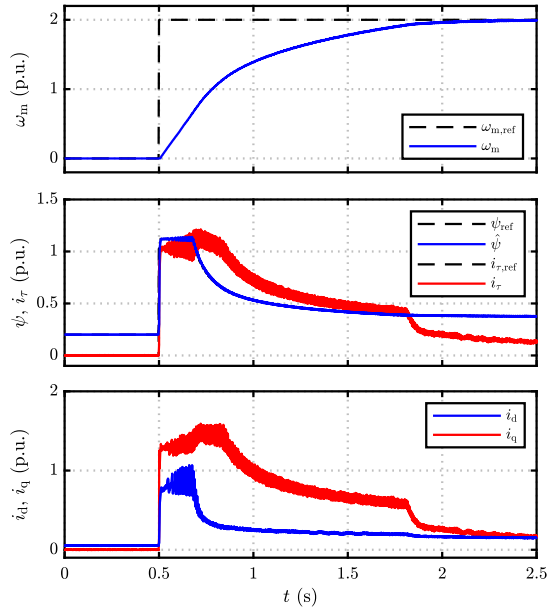

(b) Proposed controller.

Fig. 8. Experimental results showing an acceleration test for the 6.7-kW SyRM: (a) conventional controller; (b) proposed controller. First subplot: actual speed and its reference. Second subplot: controlled variables and their references. Last subplot: measured current components in rotor coordinates.

p.u., and the torque reference is stepped from 0 to the rated torque with the increments of 25% of the rated torque. Fig. 11(a,b) shows the results for the conventional controller and Fig. 11(c,d) for the proposed controller. The actual motor parameters are $L_q = 0.5\hat{L}_q$ and $\psi_f = 2\hat{\psi}_f$ in Fig. 11(a,c) and $L_q = 2\hat{L}_q$ and $\psi_f = 0.5\hat{\psi}_f$ in Fig. 11(b,d). It can be seen that there are overshoots in the controlled variables in the case of the conventional controller. Furthermore, the control system becomes unstable in the high-torque region in Fig. 11(b). In the case of the proposed controller, only minor overshoots in the controlled variables can be seen.

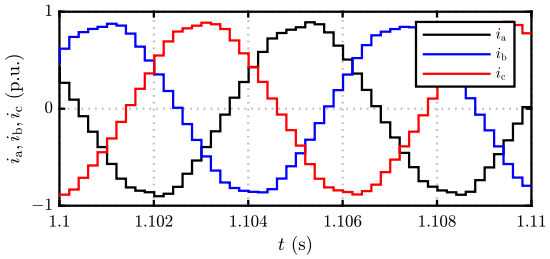

(a) Conventional controller.

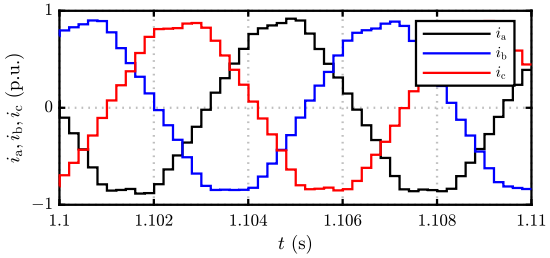

(b) Proposed controller.

Fig. 9. Phase current waveforms from the experiment in Fig. 8 with a zoomed-in time scale: (a) conventional controller; (b) proposed controller. The staircase waveforms are due to the sampling frequency of 5 kHz used in the control system.

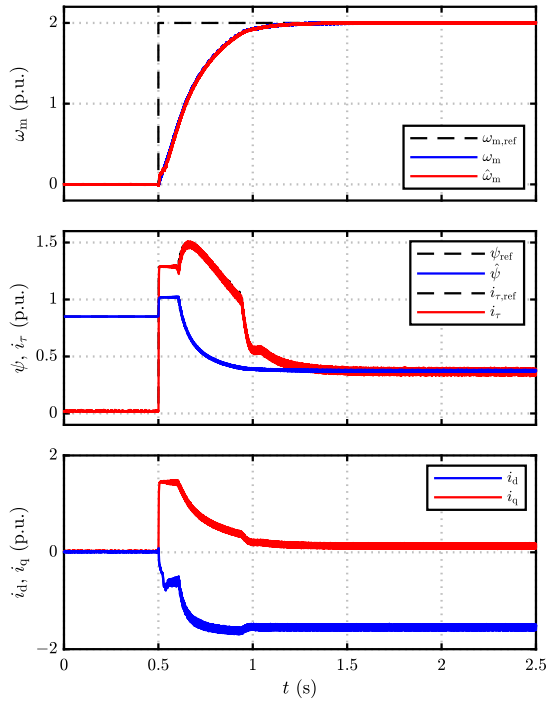

Fig. 10. Experimental results showing an acceleration test for the 2.2-kW PM motor. In this example, a motion-sensorless variant of the proposed control system is used.

The effects of the errors in L_d were also studied, but are not shown here for brevity. The proposed controller is less sensitive to the errors in L_d as well. To conclude, the proposed stator-flux-oriented-controller is more robust against parameter errors than the conventional controller.

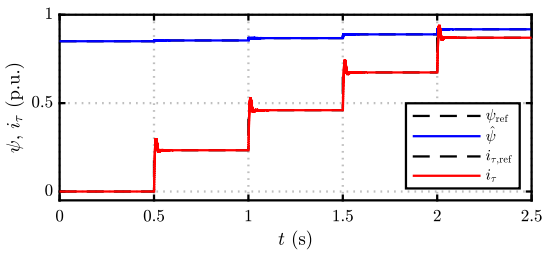

(a) Conventional: $L_{\mathrm{q}} = 0.5\hat{L}_{\mathrm{q}}$, $\psi_{\mathrm{f}} = 2\hat{\psi}_{\mathrm{f}}$.

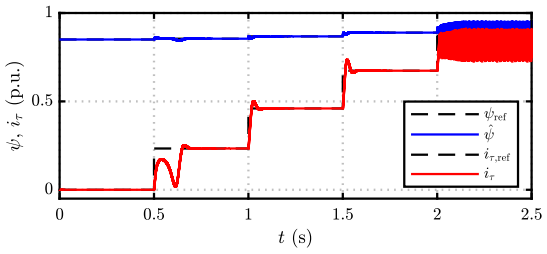

(b) Conventional: $L_{\mathrm{q}} = 2\hat{L}_{\mathrm{q}}$, $\psi_{\mathrm{f}} = 0.5\hat{\psi}_{\mathrm{f}}$.

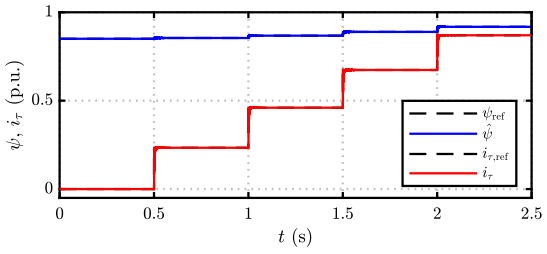

(c) Proposed: $L_{\mathrm{q}} = 0.5\hat{L}_{\mathrm{q}}$, $\psi_{\mathrm{f}} = 2\hat{\psi}_{\mathrm{f}}$.

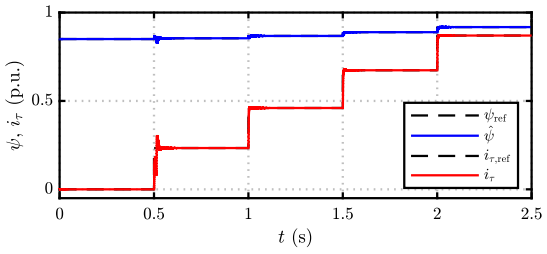

(d) Proposed: $L_{\mathrm{q}} = 2\hat{L}_{\mathrm{q}}$, $\psi_{\mathrm{f}} = 0.5\hat{\psi}_{\mathrm{f}}$.

Fig. 11. Simulation results for the 2.2-kW PM motor with parameter errors: (a,b) conventional controller; (c,d) proposed controller. The torque is changed stepwise at the constant speed of $\omega_{\mathrm{m}} = 0.75$ p.u. The actual motor parameters are given in the subcaptions (and $L_{\mathrm{d}} = \hat{L}_{\mathrm{d}}$ in all the cases).

B. Summary of Key Features

As discussed in Sections I and III, much simpler reference calculation methods can be used for stator-flux-oriented control than for rotor-oriented current control. Typically, a current-controlled drive system requires at least one two-dimensional look-up table (in addition to the MTPA and MTPV look-up tables), which is computed off-line using a complicated special algorithm [4], [6]. Furthermore, two-dimensional look-up tables require more memory in the embedded processor and interpolation algorithms increase the computational burden.

As mentioned in Section III, the MTPV limit as well as the zero-flux condition are singularities in stator-flux-oriented control. These singularities can be easily avoided with negligible losses in the energy efficiency and in the maximum torque capability. In the case of current-controlled drives, these singularities do not exist. Furthermore, the current limitation is easier to implement in the current-controlled drives.

The robustness of a current-controlled drive and of a stator-flux-orientation controlled drive against parameter errors is similar, if their closed-loop poles are placed similarly and if the sampling frequencies are high enough. If a very low ratio of the sampling frequency to the maximum speed is required, the robustness of current control can be further improved by means of the direct discrete-time control design [8], [22], while this design option is not yet available for stator-flux-oriented control.

For controlling highly saturated machines (such as SyRMs), the magnetic saturation model can be incorporated into the stator-flux-oriented controller, as was done in the experimental systems of this paper. Compared to the standard current controller with the same magnetic model, the proposed stator-flux-oriented controller works better in transients, since the flux magnitude is used as another controlled state variable. Even better robustness against the magnetic saturation can be achieved by applying the flux-linkage-based current controller, where the d- and q-axis flux components are controlled [10]. However, this method shares the drawback of the standard current control, i.e., a more complicated reference calculation method is needed. To summarize, the simplicity and robustness of stator-flux-oriented control is tempting for the vast majority of the applications, while more complicated methods may bring benefits in some special applications.

VI. Conclusions

We have presented a systematic design procedure for a decoupled stator-flux-oriented control method for synchronous motors. The stator-flux-oriented controller makes it possible to use a comparatively simple reference calculation scheme. However, its torque-producing current control loop is nonlinear, which makes designing the controller difficult. An exact input-output feedback linearization scheme is developed and combined with a simple linear control law. Only one design parameter, the closed-loop bandwidth, is needed. Furthermore, to prevent integrator windup, the controller is equipped with an anti-windup scheme based on the realizable reference, taking into account the nonlinear structure of the controller. As compared to the conventional controller, the proposed controller provides better dynamic performance, is more robust against parameter errors, and is easier to tune. The performance of the proposed controller has been verified using experiments, both in the motion-sensored and motion-sensorless operation.

Appendix
Data of the Motor Drives

The data of the 6.7-kW four-pole SyRM at the rated operating point are given in Table I and the saturation characteristics are shown in Fig. 12. The effects of the magnetic saturation are taken into account in the control system by replacing the flux model in (2) with an algebraic magnetic model [28].

TABLE I
DATA OF THE 6.7-KW SYRM

Rated values		
Phase voltage (peak value)	$\sqrt{2/3}$·370 V	1.00 p.u.
Current (peak value)	$\sqrt{2}$·15.5 A	1.00 p.u.
Frequency	105.8 Hz	1.00 p.u.
Speed	3 175 r/min	1.00 p.u.
Torque	20.1 Nm	0.67 p.u.
Parameters at the rated operating point		
d-axis inductance L_d	46 mH	2.20 p.u.
q-axis inductance L_q	6.8 mH	0.33 p.u.
Stator resistance R	0.55 Ω	0.04 p.u.

TABLE II
DATA OF THE 2.2-KW INTERIOR PM SYNCHRONOUS MOTOR

Rated values		
Phase voltage (peak value)	$\sqrt{2/3}$·370 V	1.00 p.u.
Current (peak value)	$\sqrt{2}$·4.3 A	1.00 p.u.
Frequency	75 Hz	1.00 p.u.
Speed	1 500 r/min	1.00 p.u.
Torque	14 Nm	0.80 p.u.
Parameters at the rated operating point		
d-axis inductance L_d	36 mH	0.34 p.u.
q-axis inductance L_q	51 mH	0.48 p.u.
Stator resistance R	3.6 Ω	0.07 p.u.
PM flux linkage ψ_f	0.55 Vs	0.85 p.u.

The data of the 2.2-kW six-pole interior PM synchronous motor is given in Table II. The magnetic saturation of this PM motor is minor, even at very high current values. Therefore, the constant inductances given in Table II are used in the control system. Both motors are fed by a 400-V 31-A inverter.

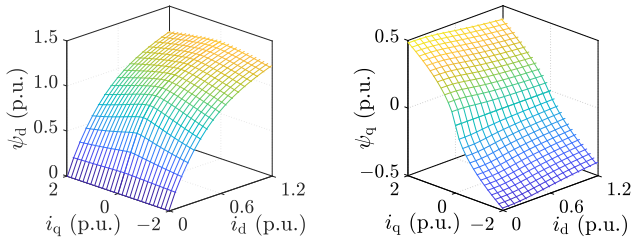

(a) (b)

Fig. 12. Saturation characteristics of a 6.7-kW SyRM: (a) $\psi_\mathrm{d} = \psi_\mathrm{d}(i_\mathrm{d}, i_\mathrm{q})$; (b) $\psi_\mathrm{q} = \psi_\mathrm{q}(i_\mathrm{d}, i_\mathrm{q})$.

REFERENCES

[1] S. Morimoto, Y. Takeda, T. Hirasa, and K. Taniguchi, "Expansion of operating limits for permanent magnet motor by current vector control considering inverter capacity," *IEEE Trans. Ind. Appl.*, vol. 26, no. 5, pp. 866–871, Sep./Oct. 1990.

[2] B.-H. Bae, N. Patel, S. Schulz, and S.-K. Sul, "New field weakening technique for high saliency interior permanent magnet motor," in *Conf. Rec. IEEE-IAS Annu. Meeting*, vol. 2, Salt Lake City, UT, Oct. 2003, pp. 898–905.

[3] M. Meyer and J. Böcker, "Optimum control for interior permanent magnet synchronous motors (IPMSM) in constant torque and flux weakening range," in *Proc. EPE-PEMC*, Portoroz, Slovenia, Aug./Sep. 2006, pp. 282–286.

[4] B. Cheng and T. R. Tesch, "Torque feedforward control technique for permanent-magnet synchronous motors," *IEEE Trans. Ind. Electron.*, vol. 57, no. 3, pp. 969–974, Mar. 2010.

[5] W. Peters, O. Wallscheid, and J. Böcker, "Optimum efficiency control of interior permanent magnet synchronous motors in drive trains of electric and hybrid vehicles," in *Proc. EPE ECCE-Europe*, Geneva, Switzerland, Sep. 2015.

[6] H. A. A. Awan, Z. Song, S. E. Saarakkala, and M. Hinkkanen, "Optimal torque control of saturated synchronous motor drives: Plug-and-play method," *IEEE Trans. Ind. Appl.*, vol. 54, no. 6, pp. 6110–6120, Nov./Dec. 2018.

[7] H. Kim, M. W. Degner, J. M. Guerrero, F. Briz, and R. D. Lorenz, "Discrete-time current regulator design for AC machine drives," *IEEE Trans. Ind. Appl.*, vol. 46, no. 4, pp. 1425–1435, Jul./Aug. 2010.

[8] M. Hinkkanen, H. A. A. Awan, Z. Qu, T. Tuovinen, and F. Briz, "Current control for synchronous motor drives: direct discrete-time pole-placement design," *IEEE Trans. Ind. Appl.*, vol. 52, no. 2, pp. 1530–1541, Mar./Apr. 2016.

[9] A. Altomare, A. Guagnano, F. Cupertino, and D. Naso, "Discrete-time control of high-speed salient machines," *IEEE Trans. Ind. Appl.*, vol. 52, no. 1, pp. 293–301, Jan./Feb. 2016.

[10] H. A. A. Awan, S. E. Saarakkala, and M. Hinkkanen, "Flux-linkage-based current control of saturated synchronous motors," *IEEE Trans. Ind. Appl.*, 2019, early access.

[11] F. Briz and M. Hinkkanen, "Design, implementation and performance of synchronous current regulators for AC drives," *Chinese Journal of Electrical Engineering*, vol. 4, no. 3, pp. 53–65, Sep. 2018.

[12] I. Takahashi and T. Noguchi, "A new quick-response and high-efficiency control strategy of an induction motor," *IEEE Trans. Ind. Appl.*, vol. 22, no. 5, pp. 820–827, Sep./Oct. 1986.

[13] G. S. Buja and M. P. Kazmierkowski, "Direct torque control of PWM inverter-fed AC motors—a survey," *IEEE Trans. Ind. Electron.*, vol. 51, no. 4, pp. 744–757, Aug. 2004.

[14] A. Tripathi, A. M. Khambadkone, and S. K. Panda, "Torque ripple analysis and dynamic performance of a space vector modulation based control method for ac-drives," *IEEE Trans. Power Electron.*, vol. 20, no. 2, pp. 485–492, Mar. 2005.

[15] Y. Inoue, S. Morimoto, and M. Sanada, "Comparative study of PMSM drive systems based on current control and direct torque control in flux-weakening control region," *IEEE Trans. Ind. Appl.*, vol. 48, no. 6, pp. 2382–2389, Nov./Dec. 2012.

[16] M. Bilewski, A. Fratta, L. Giordano, A. Vagati, and F. Villata, "Control of high-performance interior permanent magnet synchronous drives," *IEEE Trans. Ind. Appl.*, vol. 29, no. 2, pp. 328–337, Mar./Apr. 1993.

[17] H. F. Hofmann, S. R. Sanders, and A. EL-Antably, "Stator-flux-oriented vector control of synchronous reluctance machines with maximized efficiency," *IEEE Trans. Ind. Electron.*, vol. 51, no. 5, pp. 1066–1072, Oct. 2004.

[18] G. Pellegrino, E. Armando, and P. Guglielmi, "Direct flux field-oriented control of IPM drives with variable DC link in the field-weakening region," *IEEE Trans. Ind. Appl.*, vol. 45, no. 5, pp. 1619–1627, Sep./Oct. 2009.

[19] ——, "Direct-flux vector control of IPM motor drives in the maximum torque per voltage speed range," *IEEE Trans. Ind. Electron.*, vol. 59, no. 10, pp. 3780–3788, Oct. 2012.

[20] S. Ekanayake, R. Dutta, M. F. Rahman, and D. Xiao, "Direct torque and flux control of interior permanent magnet synchronous machine in deep flux-weakening region," *IET Electr. Power Appl.*, vol. 12, no. 1, pp. 98–105, Jan. 2018.

[21] M. Moradian, J. Soltani, A. Najjar-Khodabakhsh, and G. A. Markadeh, "Adaptive torque and flux control of sensorless IPMSM drive in the stator flux field oriented reference frame," *IEEE Trans. Ind. Informat.*, vol. 15, no. 1, pp. 205–212, Jan. 2019.

[22] H. A. A. Awan, M. Hinkkanen, R. Bojoi, and G. Pellegrino, "Stator-flux-oriented control of synchronous motors: Design and implementation," in *Proc. IEEE ECCE*, Portland, OR, Sep. 2018, pp. 6571–6577.

[23] P. Guglielmi, M. Pastorelli, G. Pellegrino, and A. Vagati, "Position-sensorless control of permanent-magnet-assisted synchronous reluctance motor," *IEEE Trans. Ind. Appl.*, vol. 40, no. 2, pp. 615–622, Mar./Apr. 2004.

[24] M. Hinkkanen, S. E. Saarakkala, H. A. A. Awan, E. Mölsä, and T. Tuovinen, "Observers for sensorless synchronous motor drives: Framework for design and analysis," *IEEE Trans. Ind. Appl.*, vol. 54, no. 6, pp. 6090–6100, Nov./Dec. 2018.

[25] S. S. Sastry and A. Isidori, "Adaptive control of linearizable systems," *IEEE Trans. Autom. Control*, vol. 34, no. 11, pp. 1123–1131, Nov. 1989.

[26] A. M. Khambadkone and J. Holtz, "Compensated synchronous PI current controller in overmodulation range and six-step operation of space-vector-modulation based vector-controlled drives," *IEEE Trans. Ind. Electron.*, vol. 49, no. 3, pp. 574–580, Jun. 2002.

[27] Y. Peng, D. Vrancic, and R. Hanus, "Anti-windup, bumpless, and conditioned transfer techniques for PID controllers," *IEEE Control Syst. Mag.*, vol. 16, no. 4, pp. 48–57, Aug. 1996.

[28] M. Hinkkanen, P. Pescetto, E. Mölsä, S. E. Saarakkala, G. Pellegrino, and R. Bojoi, "Sensorless self-commissioning of synchronous reluctance motors at standstill without rotor locking," *IEEE Trans. Ind. Appl.*, vol. 53, no. 3, pp. 2120–2129, May/Jun. 2017.

Hafiz Asad Ali Awan received the B.Sc. degree in electrical engineering from the University of Engineering and Technology, Lahore, Pakistan, in 2012, and the M.Sc.(Tech.) degree in electrical engineering from Aalto University, Espoo, Finland, in 2015. He is working toward the D.Sc.(Tech.) degree at Aalto University.

He is currently a Design Engineer with ABB Oy Drives, Helsinki, Finland. His main research interest include control of electric drives.

Mr. Awan was the co-recipient of the 2018 IEEE Industry Applications Society Industrial Drives Committee Best Paper Award.

Marko Hinkkanen (M'06–SM'13) received the M.Sc.(Eng.) and D.Sc.(Tech.) degrees in electrical engineering from the Helsinki University of Technology, Espoo, Finland, in 2000 and 2004, respectively.

He is an Associate Professor with the School of Electrical Engineering, Aalto University, Espoo. His research interests include control systems, electric drives, and power converters.

Dr. Hinkkanen was a General Co-Chair for the 2018 IEEE 9th International Symposium on Sensorless Control for Electrical Drives (SLED). He was the co-recipient of the 2016 International Conference on Electrical Machines (ICEM) Brian J. Chalmers Best Paper Award and the 2016 and 2018 IEEE Industry Applications Society Industrial Drives Committee Best Paper Awards. He is an Associate Editor of the *IEEE Transactions on Energy Conversion* and of *IET Electric Power Applications*.

Radu Bojoi (M'06–SM'10–F'19) received the M.Sc. degree in electrical engineering from the Technical University of Iasi, Romania, in 1993, and the Ph.D. degree in electrical engineering from the Politecnico di Torino, Italy, in 2002, where he is currently a Full Professor of power electronics and electrical drives and the Director of the Power Electronics Innovation Center.

He has published more than 150 papers covering power electronics and electrical drives for industrial applications, transportation electrification, power quality, and home appliances. He was involved in many research projects with industry for direct technology transfer aiming at obtaining new products.

Dr. Bojoi was the co-recipient of five prize paper awards, the last one as the IEEE-IAS Prize Paper Award, in 2015. He is an Associate Editor of the *IEEE Transactions on Industrial Electronics*.

Gianmario Pellegrino o (M'06–SM'13) received the Ph.D. degree in electrical engineering from Politecnico di Torino, Turin, Italy, in 2002.

He is an Associate Professor of Electrical Machines and Drives at the Politecnico di Torino, Turin. He was a Visiting Fellow with Aalborg University, Denmark, the University of Nottingham, U.K., and the University of Wisconsin-Madison, USA. He has authored and coauthored 40 IEEE journal papers and one patent. He is a member of the Power Electronics Interdepartmental Laboratory (PEIC) established in 2017 at the Politecnico di Torino and a member of the Advisory Board of PCIM Europe. He is currently the Vice President of the CMAEL Association, representative of the scholars in Power Converters, Electrical Machines, and Drives in Italy, and the Rector's Advisor for Interdepartmental Centers of Politecnico di Torino. He is one of the authors of the open-source project SyR-e for the design of electrical motors and engaged in several research projects with the industry.

Dr. Pellegrino is an Associate Editor for the *IEEE Transactions on Industry Applications* and was the recipient of seven Best Paper Awards.